

Time-dependent Goos-Hänchen Shifts in Gapped Graphene

Bouchaib Lemaalem^a, Miloud Mekkaoui^a, Ahmed Jellal^{*a} and Hocine Bahlouli^b

^a*Laboratory of Theoretical Physics, Faculty of Sciences, Chouaib Doukkali University,
PO Box 20, 24000 El Jadida, Morocco*

^b*Physics Department, King Fahd University of Petroleum & Minerals,
Dhahran 31261, Saudi Arabia*

Abstract

We study the Goos-Hänchen (GH) shifts for transmitted Dirac fermions in gapped graphene through a single barrier structure having a time periodic oscillating component. Our analysis shows that the GH shifts in transmission for central band $l = 0$ and two first sidebands $l = \pm 1$ change sign at the Dirac points $E = V + l\hbar\omega$. In particular the GH shifts in transmission exhibit enhanced peaks at each bound state associated with the single barrier when the incident angle is less than the critical angle associated with total reflection. Klein tunneling, reflected by perfect transmission at normal incidence, is also preserved in the presence of an oscillating barrier.

PACS numbers: 73.63.-b; 73.23.-b; 72.80.Rj

Keywords: Graphene, time-oscillating barrier, Dirac equation, Goos-Hänchen shifts.

*a.jellal@ucd.ac.ma

1 Introduction

When a light beam experiences a total reflection at the interface of two media having different indices of refraction it shifts along the interface by a certain distance. Such a lateral displacement between the incident and reflected beams is called the Goos-Hänchen (GH) effect [1]. Since the transport carriers in graphene behave like massless particles, then by analogy with light, GH shift has been investigated in various graphene based nanostructure devices. It has also been found that the GH shift can be enhanced by the presence of transmission resonances [2–4] while its control can be achieved through tunability of the applied electrostatic potential and induced gap [2,5]. It has been found that the GH shift plays an important role in the group velocity of quasiparticles along interfaces of graphene p-n junctions [6,7].

Time dependent phenomena and in particular periodic fields and oscillating potential barriers play an important role in nanostructure devices. For instances, the application of a periodic oscillating electromagnetic field gives rise to additional side band resonant energies at $E + l\hbar\omega$ ($l = 0, \pm 1, \dots$) in the transmission probability [8,9]. These resonant energies originate from the fact that electrons while interacting with the oscillating field will exchange photons of energy $\hbar\omega$, ω being the frequency of the oscillating magnetic field. Dayem and Martin [10] were the first to provide evidence of photon assisted tunneling when they subjected a thin superconducting film to a microwave field. Subsequently, Tien and Gordon [11] used a time modulated scalar potential as a theoretical model to explain these experimental observations. Further theoretical studies were performed later by other research groups, in particular Buttiker and Landauer investigated the barrier traversal time of particles interacting with a time-oscillating barrier [12]. Then Wagner and other workers [13] gave a detailed treatment on photon-assisted transport through quantum wells and barriers with oscillating potentials and studied in depth the transmission probability as a function of the potential parameters.

In our previous work [9] we have analyzed the energy spectrum together with the corresponding transmission in graphene through a square potential barrier driven by a periodic potential. In the present work we consider the same system but with a gap and study and study the transport of Dirac fermions. The barrier height oscillates sinusoidally around an average value V_j with oscillation amplitude U_j and frequency ω . Thus we will investigate the negative and positive GH shifts in transmission for the central band and sidebands of Dirac fermions through a time-oscillating potential in monolayer graphene, based on the tunable transmission gap [2,14]. The GH shifts for the central band and first sidebands discussed here are related to the transmission resonances, which are quite different from the GH shift for total reflection at a single graphene interface. Using the derived energy spectrum we compute the GH shifts for the central and sidebands and study their variations in terms of the system physical parameters and phase shifts. To give a better understanding of our results, we perform a numerical study based on various choices of the physical parameters. Among the obtained results we show that GH shifts in transmission can be controlled by a square potential barrier harmonically oscillating in time. It is worth mentioning that few recent references have considered the GH shifts due to irradiation of graphene sheet with a time-dependent oscillating magnetic field [15]. Others investigated the GH shifts in a strained graphene sheet where the mechanical strain is described by a gauge vector potential giving rise to a pseudo-magnetic field that affected differently the valley [16].

The work is organized as follows. In section 2, we use the solutions of the energy spectrum associated with our system together with transmission probabilities to determine the GH shifts. We numerically analyze and discuss the GH shifts in transmission within the central band and first sidebands by considering suitable choices of the physical parameters in section 3. Conclusions are given in last section.

2 Goos-Hänshen shifts

Opening and controlling a band gap in graphene is one of the most important issues that need to be resolved with certitude to ensure the usage of graphene in telecommunication or information technology. Several methods have been advanced to create such band gap in graphene such as deposition of graphene on a well selected substrate having a similar honeycomb structure [17], application of strain [18] or creation of nanoribbons by physically cutting the graphene sheet giving rise to an effective mass [19]. However the existence of a substrate induced energy gap in graphene due to its interaction with substrate SiC or BN is still debatable [20]. Setting aside the issue of existence and realization of an energy gap in graphene while preserving its honeycomb lattice symmetry, we consider in our model a gapped graphene subject to a square potential barrier of width d and oscillating sinusoidally around its average height V_j with amplitude U_j and frequency ω . Fermions with energy E are incident from one side of the barrier at incidence angle ϕ_0 with respect to the x -axis and leave the barrier with energy $E + m\hbar\omega$ ($m = 0, \pm 1, \pm 2, \dots$) making angles $\pi - \phi_m$ after reflection and ϕ_m after transmission. The corresponding Hamiltonian is

$$H_j = -i\hbar v_F \vec{\sigma} \cdot \vec{\nabla} + \Delta \sigma_z + [V_j(x) + U_j \cos(\omega t)] \mathbb{I}_2 \quad (1)$$

where v_F is the Fermi velocity, $\sigma = (\sigma_x, \sigma_y)$ are the Pauli matrices, \mathbb{I}_2 is the 2×2 unit matrix, V is the static square potential barrier and U_j is the amplitude of the oscillating potential, both of which are constant for $0 \leq x \leq d$, with d positive, and zero elsewhere (Figure 1)

$$V_j(x) = \begin{cases} V, & 0 \leq x \leq d \\ 0, & \text{otherwise} \end{cases}, \quad U_j = \begin{cases} u_1, & 0 \leq x \leq d \\ 0, & \text{otherwise} \end{cases} \quad (2)$$

The subscript $j = 0, 1, 2$ denotes each scattering region from left to right as shown in Figure 1. The parameter $\Delta = mv_F^2$ is the energy gap owing to the sublattice symmetry breaking.

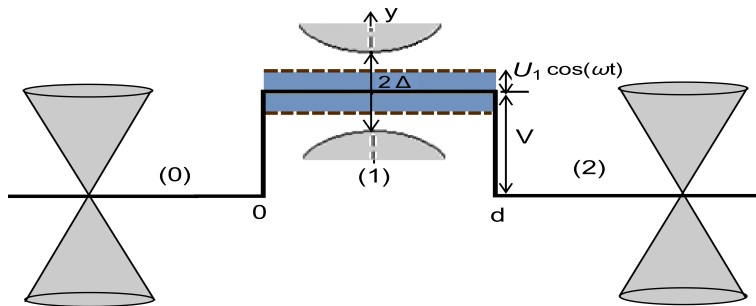


Figure 1: Schematic of the potential profile showing a time oscillating potential in a gapped graphene region subject to an electrostatic potential.

After rescaling $\epsilon = E/v_F$, $v_j = V_j/v_F$, $\mu = \Delta/v_F$, $\varpi = \omega/v_F$, $u_j = U_j/v_F$, $\alpha_1 = \frac{u_1}{\varpi}$ and taking $\hbar = 1$, we solve the Dirac equation in the three regions. In the incident region $j = 0$ ($x < 0$):

$$\psi_0(x, y, t) = e^{ik_y y} \sum_{m,l=-\infty}^{+\infty} \left[\delta_{l,0} \begin{pmatrix} 1 \\ z_l \end{pmatrix} e^{ik_l x} + r_l \begin{pmatrix} 1 \\ -\frac{1}{z_l} \end{pmatrix} e^{-ik_l x} \right] \delta_{m,l} e^{-iv_F(\epsilon+m\varpi)t} \quad (3)$$

where $z_l = s_l \frac{k_l + ik_y}{\sqrt{k_l^2 + k_y^2}}$ and $s_l = \text{sgn}(\epsilon + l\varpi)$. In the transmitted region $j = 2$ ($x > d$):

$$\psi_2(x, y, t) = e^{ik_y y} \sum_{m,l=-\infty}^{+\infty} \left[t_l \begin{pmatrix} 1 \\ z_l \end{pmatrix} e^{ik_l x} + b_l \begin{pmatrix} 1 \\ -\frac{1}{z_l} \end{pmatrix} e^{-ik_l x} \right] \delta_{m,l} e^{-iv_F(\epsilon+m\varpi)t} \quad (4)$$

where $\{b_l\}$ is the null vector. In the scattering region $j = 1$ ($0 < x < d$):

$$\psi_1(x, y, t) = e^{ik_y y} \sum_{m,l=-\infty}^{m,l=+\infty} \left[a_l^j \begin{pmatrix} c_+ \\ c_- z'_l \end{pmatrix} e^{ik'_l x} + b_l^j \begin{pmatrix} c_+ \\ -\frac{c_-}{z'_l} \end{pmatrix} e^{-ik'_l x} \right] J_{m-l}(\alpha_1) e^{-iv_F(\epsilon+m\varpi)t} \quad (5)$$

where $c_{\pm} = \sqrt{1 \pm \frac{s'_l \mu}{\sqrt{(k'_l)^2 + k_y^2}}}$, $z'_l = s'_l \frac{k'_l + ik_y}{\sqrt{(k'_l)^2 + k_y^2}}$ and the associated energy $(\epsilon - v + l\varpi)^2 - \mu^2 = s'_l \sqrt{(k'_l)^2 + k_y^2}$, with $s'_l = \text{sgn}(\epsilon + l\varpi - v)$ and $J_m(\alpha_1)$ is the Bessel function of the first kind such that $J_{m-l}(\alpha_1) = \delta_{m,l}$.

The transmission and reflection probabilities can be obtained using the continuity of the spinor wavefunctions at junction interfaces ($x = 0, x = d$), namely $\psi_0(0, y, t) = \psi_1(0, y, t)$ and $\psi_1(d, y, t) = \psi_2(d, y, t)$. These boundary conditions can be represented in matrix form as

$$\begin{pmatrix} \Xi_0 \\ \Xi'_0 \end{pmatrix} = \begin{pmatrix} \mathbb{M}_{11} & \mathbb{M}_{12} \\ \mathbb{M}_{21} & \mathbb{M}_{22} \end{pmatrix} \begin{pmatrix} \Xi_2 \\ \Xi'_2 \end{pmatrix} = \mathbb{M} \begin{pmatrix} \Xi_2 \\ \Xi'_2 \end{pmatrix} \quad (6)$$

and the total transfer matrix $\mathbb{M} = \mathbb{M}(0, 1) \cdot \mathbb{M}(1, 2)$ with

$$\mathbb{M}(0, 1) = \begin{pmatrix} \mathbb{I} & \mathbb{I} \\ \mathbb{N}^+ & \mathbb{N}^- \end{pmatrix}^{-1} \begin{pmatrix} \mathbb{C}_1 & \mathbb{C}_1 \\ \mathbb{G}_1^+ & \mathbb{G}_1^- \end{pmatrix}, \quad \mathbb{M}(1, 2) = \begin{pmatrix} \mathbb{C}_2^+ & \mathbb{C}_2^- \\ \mathbb{G}_2^+ & \mathbb{G}_2^- \end{pmatrix}^{-1} \begin{pmatrix} \mathbb{I} & \mathbb{I} \\ \mathbb{N}^+ & \mathbb{N}^- \end{pmatrix} \begin{pmatrix} \mathbb{K}^+ & \mathbb{O} \\ \mathbb{O} & \mathbb{K}^- \end{pmatrix} \quad (7)$$

where we have set the parameters $(\mathbb{N}^{\pm})_{m,l} = \pm(z_m)^{\pm 1} \delta_{m,l}$, $(\mathbb{C}_1^{\pm})_{m,l} = \alpha_1 J_{m-l}(\frac{u_1}{\varpi})$, $(\mathbb{G}_1^{\pm})_{m,l} = \pm \beta_l (z'_l)^{\pm 1} J_{m-l}(\frac{u_1}{\varpi})$, $(\mathbb{C}_2^{\pm})_{m,l} = \alpha_l e^{\pm ik'_l d} J_{m-l}(\frac{u_1}{\varpi})$, $(\mathbb{G}_2^{\pm})_{m,l} = \pm \beta_l (z'_l)^{\pm 1} e^{\pm ik'_l d} J_{m-l}(\frac{u_1}{\varpi})$, $(\mathbb{K}^{\pm})_{m,l} = \pm e^{\pm idk_l} \delta_{m,l}$ and the null matrix is denoted by \mathbb{O} , \mathbb{I} is the unit matrix.

To proceed further, we assume an electron propagating from left to right with the quasienergy $\epsilon = \frac{E}{v_F}$. Then, $\tau = (1, 2)$, $\Xi_0 = \{\delta_{0,l}\}$ and $\Xi'_2 = \{a_m\}$ is the null vector, whereas $\Xi_2 = \{t_l\}$ and $\Xi'_0 = \{r_l\}$ are the vectors for transmitted and reflected waves, respectively, $\Xi_2 = (\mathbb{M}_{11})^{-1} \cdot \Xi_0$. The minimum number N of sidebands that need to be considered is determined by the strength of the perturbing potential oscillation, $N > \frac{u_1}{\varpi}$. The infinite series for T can be then truncated to consider only a finite number of terms starting from $-N$ up to N . Furthermore, analytical results are obtained if we consider small values of $\alpha_1 = \frac{u_1}{\varpi}$ and include only the first two sidebands at energies $\epsilon \pm \varpi$ along with the central band at energy ϵ

$$t_{-N+k} = \mathbb{M}'[k+1, N+1] \quad (8)$$

where $k = 0, 1, 2, \dots, 2N$ and \mathbb{M}' is a matrix element of \mathbb{M}_{11}^{-1} . Using the reflected J^{re} and transmitted J^{tr} currents, the reflection R_l and transmission T_l probabilities for a given mode l can be expressed as

$$T_l = \frac{k_l}{k_0} |t_l|^2, \quad R_l = \frac{k_l}{k_0} |r_l|^2 \quad (9)$$

such that T_l is the probability amplitude describing the scattering of an electron with incident quasienergy E in the region 0 into the sideband with quasienergy $E + l\hbar\omega$ in the region 1. Thus, the rank of the transfer matrix \mathbb{M} increases with the amplitude of the time-oscillating potential. The amplitudes t_l and r_l can be written in complex notation as $t_l = \rho_l^t e^{i\varphi_l^t}$, $r_l = \rho_l^r e^{i\varphi_l^r}$ such that the corresponding phase shifts and moduli are defined by $\varphi_l^t = \arctan\left(\frac{t_l^* - t_l}{i(t_l^* + t_l)}\right)$, $\varphi_l^r = \arctan\left(\frac{r_l^* - r_l}{i(r_l^* + r_l)}\right)$, $\rho_l^t = \sqrt{\text{Re}^2[t_l] + \text{Im}^2[t_l]}$, $\rho_l^r = \sqrt{\text{Re}^2[r_l] + \text{Im}^2[r_l]}$, which can be used to obtain the probabilities

$$T_l = \frac{k_l}{k_0} (\text{Re}^2[t_l] + \text{Im}^2[t_l]), \quad R_l = \frac{k_l}{k_0} (\text{Re}^2[r_l] + \text{Im}^2[r_l]). \quad (10)$$

In the forthcoming analysis due to numerical difficulties, we are able to truncate (8) retaining only the terms corresponding to the central and first two sidebands, namely $l = 0, \pm 1$. We can proceed as before to derive transmission amplitudes $t_{-1} = \mathbb{M}'[1, 2]$, $t_0 = \mathbb{M}'[2, 2]$, $t_1 = \mathbb{M}'[3, 2]$. Such an approximation can be validated at low energies where two and higher-photon processes are less probable than the single photon processes.

The Goos-Hänchen shifts for Dirac fermions in gapped graphene under the applied potential can be analyzed by considering the incident, reflected and transmitted beams around some transverse wave vector $k_y = k_{y_0}$ and the angle of incidence $\phi_l(k_{y_0})$ lies in the interval $[0, \frac{\pi}{2}]$. These beams can be written in terms of the obtained solutions of the energy spectrum. Indeed, for the incident and reflected waves, we have

$$\Psi_{\text{in}}(x, y) = \int_{-\infty}^{+\infty} dk_y f(k_y - k_{y_0}) e^{i(k_0(k_y)x + k_y y)} \begin{pmatrix} 1 \\ e^{i\phi_0(k_y)} \end{pmatrix} \quad (11)$$

$$\Psi_{\text{re}}(x, y) = \int_{-\infty}^{+\infty} dk_y r_l f(k_y - k_{y_0}) e^{i(-k_l(k_y)x + k_y y)} \begin{pmatrix} 1 \\ -e^{-i\phi_l(k_y)} \end{pmatrix} \quad (12)$$

where $\phi_l = \tan^{-1} \frac{k_y}{k_l}$, ϕ_0 is the incident angle and $f(k_y - k_{y_0})$ the angular spectral distribution. We can approximate the k_y -dependent terms by a Taylor expansion around k_{y_0} , retaining only the first order term to end up with

$$\phi_l(k_y) \approx \phi_l(k_{y_0}) + \left. \frac{\partial \phi_l}{\partial k_y} \right|_{k_{y_0}} (k_y - k_{y_0}), \quad k_l(k_y) \approx k_l(k_{y_0}) + \left. \frac{\partial k_l}{\partial k_y} \right|_{k_{y_0}} (k_y - k_{y_0}). \quad (13)$$

As for the transmitted beam, we have

$$\Psi_{\text{tr}}(x, y) = \int_{-\infty}^{+\infty} dk_y t_l f(k_y - k_{y_0}) e^{i(k_l(k_y)x + k_y y)} \begin{pmatrix} 1 \\ e^{i\phi_l(k_y)} \end{pmatrix}. \quad (14)$$

The stationary-phase approximation indicates that the GH shifts are equal to the negative gradient of transmission phase with respect to k_y . To calculate the GH shifts of the transmitted beam through our system we adopt the definition from [21, 22], accordingly the stationary phase method [23] gives

$$S_l^t = - \left. \frac{\partial \varphi_l^t}{\partial k_y} \right|_{k_{y_0}}, \quad S_l^r = - \left. \frac{\partial \varphi_l^r}{\partial k_y} \right|_{k_{y_0}}. \quad (15)$$

Assuming a finite beam width with Gaussian shape, $f(k_y - k_{y0}) = w_y \exp[-w_y^2(k_y - k_{y0})^2]$ around k_{y0} , where $w_y = w \sec \phi_l$, with half beam width w at the waist, we can evaluate the Gaussian integral to obtain the spatial profile of the incident beam, by expanding ϕ_l and k_l to first order around k_{y0} when satisfying the required condition $\delta\phi_l = \lambda_F/(\pi w) \ll 1$ with the Fermi wavelength λ_F . Comparison of the incident and transmitted beams suggests that the displacements σ_{\pm} of up and down spinor components are both equal to $\partial\varphi_l^t/\partial k_{y0}$ and the average displacement is given by

$$S_l^t = \frac{1}{2}(\sigma^+ + \sigma^-) = -\left.\frac{\partial\varphi_l^t}{\partial k_y}\right|_{k_{y0}}. \quad (16)$$

Next we will numerically analyze and discuss the GH shifts for the central band S_0^t and first sidebands $S_{\pm 1}^t$ for Dirac fermions in gapped graphene scattered by a square barrier with height that oscillates sinusoidally. This will be done by selecting adequately the physical parameters characterizing our system.

3 Discussion of numerical results

To allow for a suitable interpretation of our main results, we compute numerically the GH shifts in transmission for the central band and first sidebands under various conditions. First we plot the GH shifts in transmission S_l^t as a function of the potential v of the oscillating barrier in the gapless graphene region where $\mu = 0$, the energy $\epsilon = 10$ and the frequency $\varpi = 1$, see Figure 2. It is clear that the GH shifts change sign at the Dirac points, namely $v = \epsilon + l\varpi$ with $(l = -1, 0, 1)$. We observe that S_l^t exhibit negative as well as positive values and strongly depend on the location of Dirac points. In Figure 2(a), we observe, when $d = 2.5$, $\alpha = 0.2$ and $k_y = 1$, that the GH shifts in transmission for the central band and the two first sidebands S_0^t (blue line), S_{-1}^t (green line) and S_1^t (red line) change sign at the Dirac points ϵ , $\epsilon - \varpi$ and $\epsilon + \varpi$, respectively. Figure 2(b) shows for different values of $\alpha_1 = \{0.2, 0.6, 0.9\}$, that the GH shifts for central band S_0^t in the oscillating barrier decreases if α_1 increases. This tells us that by adjusting the value of α_1 we can decrease the value of S_0^t . In Figure 2(c), we have chosen the parameters $\alpha_1 = 0.2$, $k_y = 1$ for three different values of the distance $d = 0.5$ (red line), $d = 1.5$ (green line), $d = 2.5$ (blue line) to show S_0^t behaviors. We observe that S_0^t increase if d increases and change its sign at the Dirac points $v = \epsilon$. This change in sign of the GH shifts shows clearly that they strongly depend on the strength of the barrier heights. Note that, the Dirac points represent the zero modes for Dirac operator [5] and lead to the emergence of new Dirac points, which have been discussed in different works [21, 24]. Such point separates the two regions of positive and negative refraction. In the cases of $v < \epsilon$ and $v > \epsilon$, S_0^t is, respectively, in the forward and backward directions due to the fact that the signs of group velocity are opposite. Figure 2(d) presents the numerical results of the GH shifts in transmission S_1^t for first band $l = 1$ as a function of the potential energy v for specific values of the barrier width $d = 1.5$, $\alpha_1 = 0.4$ and three different values of the wavevector $k_y = 0$ (red line), $k_y = 2$ (green line), $k_y = 4$ (blue line). We observe that S_1^t decrease if d decreases and then vanish for $k_y = 0$, that is to say for normal incidence there is no shift.

In Figure 3 we present the numerical results of the transmission probabilities and GH shifts in transmission as a function of barrier width d with $\epsilon = 10$, $v = 15$, $\mu = 0$, $\varpi = 1$, $k_y = 0, 2$. The transmission probability T_{0s} and the GH shifts S_{0s}^t for the static barrier are shown, which correspond

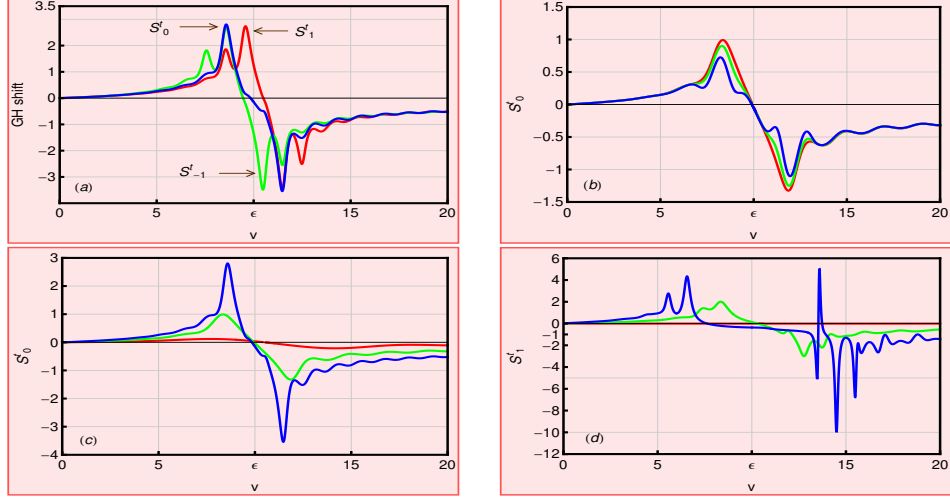


Figure 2: (color online) GH shifts in transmission S_l^t versus potential v for the oscillating barrier with $\mu = 0$, $\epsilon = 10$, $\varpi = 1$. (a): $l = -1, 0, 1$, $k_y = 1$, $d = 2.5$, $\alpha_1 = 0.2$. (b): $l = 0$, $k_y = 1$, $d = 1.5$, $\alpha_1 = 0.2$ (red line), $\alpha = 0.6$ (green line), $\alpha = 0.9$ (blue line). (c): $\alpha_1 = 0.2$, $l = 0$, $k_y = 1$, $d = 0.5$ (red line), $d = 1.5$ (green line), $d = 2.5$ (blue line). (d): $\alpha_1 = 0.4$, $l = 1$, $d = 1.5$, $k_y = 0$ (red line), $k_y = 2$ (green line), $k_y = 4$ (blue line).

to the case $\alpha_1 = \frac{\omega l}{\omega} = 0$. While for the oscillating barrier with $\alpha_1 = 0.6$, we show the GH shifts in transmission S_l^t and transmission probabilities T_l for central band $l = 0$ and first sidebands $l = \pm 1$ as a function of barrier width. The magenta, blue, green and red lines correspond to (T_{0s}, S_{0s}^t) , (T_0, S_0^t) , (T_{-1}, S_{-1}^t) and (T_1, S_1^t) , respectively. Figures 3(a,c) present the transmission probabilities and GH shifts in transmission as function of barrier width d for the wavevector $k_y = 2$ where the transmission probabilities for the central band and sidebands in the oscillating barrier show sinusoidal behaviors. We observe that the number of peaks in the GH shifts for the first sidebands S_{-1}^t and S_1^t correspond to the zero transmission probabilities for the first sidebands T_{-1} and T_1 , respectively. Figures 3(b,d) show the transmission probabilities and GH shifts in transmission for normal incidence $k_y = 0$. Obviously, T_{0s} is unity for larger barrier width and the GH shifts S_{0s}^t are zero. For the oscillating barrier, T_0 varies initially from unity and oscillates periodically for larger barrier width. However, the transmission probabilities for the other first two sidebands $T_{\pm 1}$ starts initially from zero then oscillates periodically. This occurs due to the larger tunneling time available for the electron to interact with the oscillating potential as it traverses the barrier. In addition, we find that for normal incidence in the oscillating barrier $T_{+1} = T_{-1}$ and the GH shifts $S_{\pm 1}^t = 0$. Moreover, the total transmission probability through the central band as well as the sidebands is unity. These results imply that perfect transmission at normal incidence is independent of the barrier width, which is yet another manifestation of Klein tunneling.

At this stage let us see what will happen if a gap is introduced in the intermediate region 1 ($0 \leq x \leq d$). As is shown in Figure 4 the gap affects the system energy spectrum obtained in region 1. In fact, the GH shifts S_l^t in the propagating case can be enhanced by a gap opening at the Dirac point. This has been performed by fixing the parameters $\alpha_1 = 0.5$, $k_y = 2$, $d = 1.5$, $\varpi = 1$ and making different choices for the energy and potential. For the configuration ($\epsilon = 15, v = 8$), we can still have

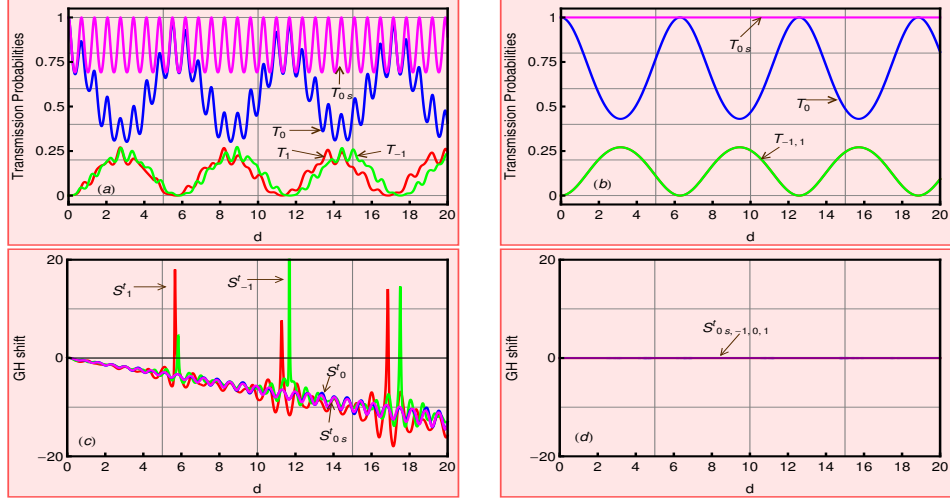


Figure 3: (color online) Transmission probability T_l and GH shifts in transmission S_l^t versus barrier width d , with $\alpha_1 = 0$ for static barrier, $\alpha_1 = 0.6$ for the oscillating barrier, $\epsilon = 10$, $v = 15$, $\mu = 0, \varpi = 1$. (a,c): $k_y = 2$ and (b,d): $k_y = 0$. For static barrier (T_{0s} , S_{0s}^t) in magenta and for oscillating barrier (T_0 , S_0^t) in blue, (T_{-1} , S_{-1}^t) in green, (T_1 , S_1^t) in red.

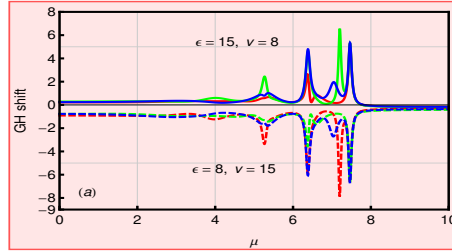


Figure 4: (color online) GH shifts in transmission S_{-1}^t (green line), S_0^t (blue line), S_{-1}^t (red line) versus energy gap μ with $\alpha_1 = 0.5$, $k_y = 2$, $d = 1.5$, $\varpi = 1$, ($\epsilon = 8, v = 15$) and ($\epsilon = 15, v = 8$).

positive shifts while for configuration ($\epsilon = 15, v = 8$) the GH shifts are negative. It is clearly seen that there are three intervals showing different behaviors of the shifts. Indeed, for $\mu \in [0, 4]$ the shifts are zero or constants according to the energy configurations, but for $\mu \in [4, 8]$ their behaviors changed completely by exhibiting some peaks and vanish in the last interval $\mu \in [8, 10]$.

Figure 5 shows the GH shifts in transmission and transmission probabilities for the central band and first two sidebands for $\alpha_1 = 0.4$ (oscillating barrier) along with that for static barrier $\alpha_1 = 0$ as a function of the potential v for specific values $k_y = 2$, $\epsilon = 10$, $\varpi = 1$ and different values of the energy gaps, see Figures 5(a,c) for $\mu = 1$ and Figures 5(b,d) for $\mu = 3$. We observe that the region of weak GH shifts becomes wide with increase in energy gap μ , the shifts are also affected by the parameters of the single barrier. In particular it changes the sign at the total reflection energies and peaks at each bound state associated with the barrier. Thus the GH shifts can be enhanced by the presence of resonant energies in the system when the incident angle is less than the critical angle associated with total reflection. It is clearly seen that S_l^t are oscillating between negative and positive values around the critical point $v = \epsilon + l\varpi$ ($l = 0, \pm 1$). At such point T_l is showing transmission probabilities for the central band and first two sidebands while it oscillates away from the critical point. We notice that

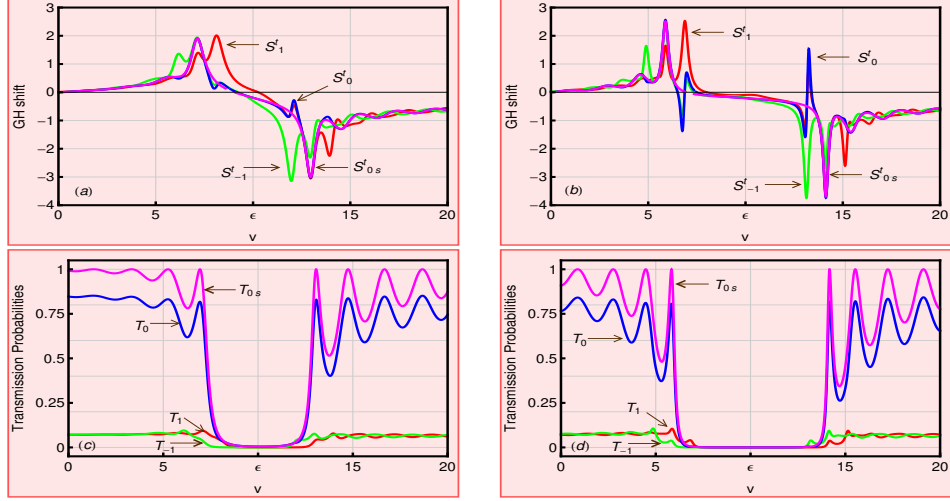


Figure 5: (color online) GH shifts in transmission and transmission probabilities for central band and first two sidebands for $\alpha_1 = 0.4$ (oscillating barrier) along with that for static barrier $\alpha_1 = 0$ as function of the potential v with $\alpha_1 = (0, 0.4)$ $k_y = 2$, $\epsilon = 10$, $d = 1.5$, $\varpi = 1$. (a,c): $\mu = 1$ and (b,d): $\mu = 3$. For static barrier (T_{0s} , S_{0s}^t) in magenta and for oscillating barrier (T_0 , S_0^t) in blue, (T_{-1} , S_{-1}^t) in green, (T_1 , S_1^t) in red.

for large values of v , the GH shifts become mostly constant and can be positive as well as negative. We deduce that there is a strong dependence of the GH shifts on the potential height v , which can help to realize a controllable sign of the GH shifts.

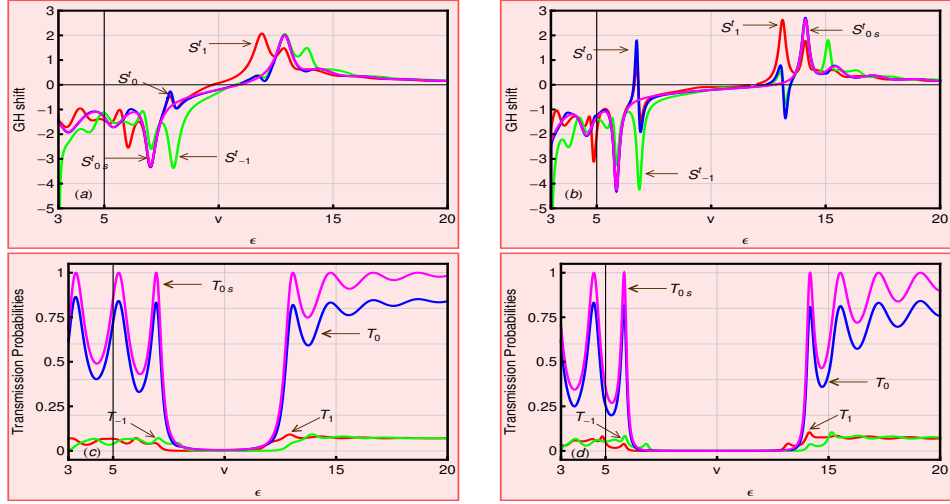


Figure 6: (color online) GH shifts in transmission S_l^t and transmission probabilities T_l as function of the incident energy ϵ with $\alpha_1 = (0, 0.4)$, $k_y = 2$, $v = 10$, $d = 1.5$, $\varpi = 1$. (a,c): $\mu = 1$ and (b,d): $\mu = 3$. For static barrier (T_{0s} , S_{0s}^t) in magenta and for oscillating barrier (T_0 , S_0^t) in blue, (T_{-1} , S_{-1}^t) in green, (T_1 , S_1^t) in red.

From Figure 6, we see that the GH shifts in transmission S_l^t and the transmission probabilities T_l versus incident energy ϵ for the values $\alpha_1 = (0, 0.4)$ $k_y = 2$, $v = 10$, $d = 1.5$, $\varpi = 1$ for two values of gap $\mu = 1$ in Figure 6(a,b) and $\mu = 3$ Figure in 6(b,d). Both quantities are showing a series of

peaks and resonances where the resonances correspond to the bound states of the static barrier for $\alpha_1 = 0$ and the oscillating barrier for $\alpha_1 = 0.4$. We notice that the GH shifts in transmission peak at each bound state energy are clearly shown in the transmission curve underneath. The energies at which transmission vanishes correspond to energies at which the GH shifts in transmission change sign. Since these resonances are very sharp (true bound states with zero width) it is numerically very difficult to track all of them, if we do then the alternation in sign of the GH shifts will be observed. We observe that around the Dirac point $\epsilon = v + l\varpi$ the number of peaks is equal to the number of transmission resonances.

4 Conclusion

We have studied the Goos-Hänchen shifts for Dirac fermions in gapped graphene through single barrier with a time periodic potential. This has been done using the solutions of the energy spectrum to write down the incident, reflected and transmitted beams in integral forms. In the second step, we have employed our results to determine the phase shifts associated with the transmission and reflection amplitudes. Subsequently, we have derived the corresponding GH shifts in terms of various physical parameters such as the width and height of the barriers, incident energy, transverse wavevector and frequency of oscillating barrier.

The time periodic electrostatic potential generates additional sidebands at energies $\epsilon + l\omega$ ($l = 0, \pm 1, \pm 2, \dots$) in the transmission probability originating from photons absorption or emission within the oscillating barrier. However, at low energies we can limit ourselves to single photon processes and neglect two photon processes. Numerically, we have shown that the GH shifts for the central band and first two sidebands depend on the incident angle of the particles, the width and height of the barrier, and the frequency of oscillation. Our results showed that the GH shifts are affected by the internal structure of the oscillating barrier. We have analyzed the GH shifts in the transmission in terms of incident energy, barrier width, potential strength and energy gap. We have observed that the GH shifts in the transmission for the central band and first two sidebands change sign at the Dirac points $\epsilon = v + l\omega$ and switch from positive to negative signs in a controllable manner. The energies at which the GH shifts in transmission change sign correspond to the sharp resonances at which the transmission vanishes. Thus, the switching of the sign of the GH shifts can be selected in a controllable manner. Then our results might provide a theoretical basis for the design of graphene based electronic switches or high sensitivity sensors based on the sign of the GH shifts.

Finally, we mention that our results could be experimentally tested using a beam splitter scanning method [25], which allows to measure the giant GH shifts produced by increasing the thicknesses of gapped graphene subject to a time oscillating potential.

Acknowledgments

The generous support provided by the Saudi Center for Theoretical Physics (SCTP) is highly appreciated by all authors. AJ and HB acknowledge the support of KFUPM under research group project RG181001.

References

- [1] F. Goos and H. Hänchen, *Ann. Phys.* 436, 333 (1947).
- [2] X. Chen, J.-W. Tao, and Y. Ban, *Eur. Phys. J. B* 79, 203 (2011).
- [3] Y. Song, H-C. Wu, and Y. Guo, *Appl. Phys. Lett.* 100, 253116 (2012).
- [4] X. Chen, P-L. Zhao, X-J. Lu, and L-G. Wang, *Eur. Phys. J. B* 86, 223 (2013).
- [5] M. Sharma and S. J. Ghosh, *J. Phys.: Condens. Matter* 23, 055501 (2011).
- [6] L. Zhao and S. F. Yelin, *Phys. Rev. B* 81, 115441 (2010).
- [7] C. W. J. Beenakker, R. A. Sepkhanov, A. R. Akhmerov, and J. Tworzydło, *Phys. Rev. Lett.* 102, 146804 (2009).
- [8] M. Ahsan Zeb, K. Sabeeh, and M. Tahir, *Phys. Rev. B* 78 (2008) 165420.
- [9] A. Jellal, M. Mekkaoui, E.B. Choubabi, and H. Bahlouli, *Eur. Phys. J. B* 87, 123 (2014).
- [10] A. H. Dayem and R. J. Martin, *Phys. Rev. Lett.* 8, 246 (1962).
- [11] P. K. Tien and J. P. Gordon, *Phys. Rev.* 129, 647 (1963).
- [12] M. Moskalets and M. Buttiker, *Phys. Rev. B* 66, 035306 (2002).
- [13] F. Grossmann, T. Dittrich, P. Jung, and P. Hanggi, *Phys. Rev. Lett.* 67, 516 (1991); M. Wagner, *Phys. Rev. B* 49, 16544 (1994); M. Wagner, *Phys. Rev. A* 51, 798 (1995).
- [14] X. Chen and J.-W. Tao, *Appl. Phys. Lett.* 94, 262102 (2009).
- [15] A. Huamn and Gonzalo Usaj, *Phys. Rev. A* 100, 033409 (2019).
- [16] Wu Zhenhua, F. Zhai, F. M. Peeters, H. Q. Xu, and Kai Chang, *Phys. Rev. Lett.* 106, 176802 (2011).
- [17] F. Guenia, M. I. Katsnelson, and A. K. Geim, *Nat. Phys.* 6, 30 (2010).
- [18] S. M. Choi, S. H. Jhi, and Y. W. Son, *Phys. Rev. B* 81, 081407 (2010).
- [19] Y. W. Son, M. L. Cohen, and S. G. Louie, *Phys. Rev. Lett.* 97, 216803 (2006).
- [20] E. Rotenberg, A. Bostwick, T. Ohta, J. L. McChesney, T. Seyller, and K. Horn, *Nat. Mat.* 8, 258 (2008).
- [21] X. Chen, J.-W. Tao, and Y. Ban, *Eur. Phys. J. B* 79, 203 (2011).
- [22] A. Jellal, Y. Wang, Y. Zahidi, and M. Mekkaoui, *Physica E* 68, 53 (2015).
- [23] D. Bohm, *Quantum Theory*, (Prentice-Hall, New York, 1951), pp. 257-261.
- [24] L.-G. Wang and S.-Y. Zhu, *Phys. Rev. B* 81, 205444 (2010).

- [25] Xin Li, Peng Wang, Fei Xing, Xu-Dong Chen, Zhi-Bo Liu, and Jian-Guo Tian, *Opt. Lett* 39, 5574 (2014).